Magnetic-field-induced transitions in multiferroic $TbMnO_3$ probed by resonant and nonresonant x-ray diffraction

J. Strempfer,[1,*] B. Bohnenbuck,[2] I. Zegkinoglou,[2] N. Aliouane,[3] S. Landsgesell,[3] M. v. Zimmermann,[1] and D. N. Argyriou[3]
[1]*Hamburger Synchrotronstrahlungslabor (HASYLAB) at Deutsches Elektronensynchrotron (DESY), 22605 Hamburg, Germany*
[2]*Max-Planck-Institut für Festkörperforschung, 70569 Stuttgart, Germany*
[3]*Helmholtz-Zentrum Berlin für Materialien und Energie, 14109 Berlin, Germany*
(Received 29 April 2008; published 23 July 2008)

Multiferroic $TbMnO_3$ is investigated using x-ray diffraction in high magnetic fields. Measurements on first- and second-harmonic structural reflections due to modulations induced by the Mn and Tb magnetic order are presented as function of temperature and field oriented along the *a* and *b* directions of the crystal. The relation to changes in ordering of the rare earth moments in applied field is discussed. Observations below T_N^{Tb} without and with applied magnetic field point to a strong interaction of the rare earth order, the Mn moments, and the lattice. Also, the incommensurate to commensurate transition of the wave vector at the critical fields is discussed with respect to the Tb and Mn magnetic order, and a phase diagram on basis of these observations for magnetic fields $H\|a$ and $H\|b$ is presented. The observations point to a complicated and delicate magnetoelastic interaction as function of temperature and field.

DOI: 10.1103/PhysRevB.78.024429 PACS number(s): 75.47.Lx, 75.50.Ee, 77.80.Bh, 78.70.Ck

I. INTRODUCTION

Magnetoelectric materials or multiferroics have stimulated much interest both scientifically and technologically—scientifically because the mechanism of coupling between ferroelectricity and magnetism is a fundamental part in understanding the properties of materials and technologically because of the flexibility of controlling states of a device with either electric or magnetic field or both. Although modern multiferroics operate at temperatures and fields prohibitive of direct applications, they offer an exciting play ground in order to better understand such coupled behavior.

Manganite perovskites $RMnO_3$, where *R* is a trivalent rare earth ion, have shown an extremely rich (H,T) phase diagram of ferroelectric and magnetic phases. Here the frustration of magnetism in $RMnO_3$ manganite perovskites[1] offers the means to break the chemical incompatibility between ferroelectricity and magnetism.[2] The tuning of the tolerance factor with appropriate size *R* ions suppresses T_N for *A*-type ordering of ferromagnetic Mn layers that are stacked antiparallel along the *c* axis and leads to low-temperature incommensurate (IC) spin ordering for $R=$Gd, Tb, and Dy.[1] For $TbMnO_3$ in particular, Mn spins order below $T_N=41$ K to form a spin density wave (SDW) with propagation vector $\tau^{\mathrm{Mn}}=\delta^{\mathrm{Mn}}\mathbf{b}^*$, $\delta^{\mathrm{Mn}}\sim 0.27$, while below $T_s=29$ K the observation of a spontaneous polarization (**P**) along the *c* axis coincides with the onset of a transverse spiral (cycloidal) ordering of Mn spins.[3] At lower temperatures there is an additional transition below $T_N^{\mathrm{Tb}}=7$ K in which Tb spins order also incommensurately with $\tau^{\mathrm{Tb}}=\delta^{\mathrm{Tb}}\mathbf{b}^*$, $\delta^{\mathrm{Tb}}=0.42$. Below T_s, neutron diffraction measurements show that the magnetic ordering is that of a transverse spiral with Mn spins rotating within the *bc* plane. Within the orthorhombic *Pbnm* crystal structure of $TbMnO_3$ ($a=5.3$ Å, $b=5.8$ Å, $c=7.4$ Å at 300 K), this ordering can be described as

$$\mathbf{M} = m_x\mathbf{x} + m_y\mathbf{y}\cos(\tau\cdot\mathbf{r}) + m_z\mathbf{z}\sin(\tau\cdot\mathbf{r}), \qquad (1)$$

where m_i represent the magnitudes of the Mn moment along the principal crystallographic directions $\mathbf{x}$, $\mathbf{y}$, $\mathbf{z}$ (a,b,c) and $\mathbf{r}$ is the position of the Mn ion. For zero field m_x is very small or zero, while below T_s the orthogonal components along $\mathbf{y}$ and $\mathbf{z}$ result in a transverse spiral ordering of Mn spins.[3] As discussed in Ref. 4, from phenomenology it follows that the ferroelectric polarization is given by

$$\mathbf{P} = \gamma\chi_e m_x m_z[e_x\times\tau], \qquad (2)$$

where χ_e is the dielectric susceptibility, γ a coupling constant, and e_x is the spin rotation axis. Since the propagation vector is parallel to the *b* axis and Mn spins rotate within the *bc* plane around the *a* axis ($e_x\|a$), the above relation predicts the direction of the polarization to be along the *c* axis, as indeed found experimentally.[5] Similarly the flop of the polarization from $P\|c$ to $P\|a$ (Ref. 5) that occurs under magnetic field applied either along the *a* or *b* axis would be expected to result from a flop of the transverse spiral from the *bc* to the *ab* plane.[4]

The incommensurate magnetic ordering in multiferroic manganites is accompanied by lattice deformations that result in structural superlattice reflections at 2τ.[1] The extinction condition in reciprocal space of these second-harmonic reflections are the same as for their magnetic $\tau=\delta\mathbf{b}^*$ counterparts. Phenomenologically the nature of these reflections is magnetostrictive and arises from a quadratic magnetoelastic coupling[6] between an amplitude modulation of the magnetic moment and the lattice. However Jia *et al.*[7] have recently discussed the spin-lattice coupling in multiferroic manganites in terms of the magnetostrictive, orbital, and Dzyaloshinskii-Moriya (DM) interactions (or $S_i\times S_j$ spin-current terms[8]) on the basis of the electronic configurations of insulating manganites. From these results it follows that for a SDW, 2τ lattice reflections are expected to be observed, while for a circular transverse spiral ($m_y=m_z$), 2τ reflections are suppressed.[7] If the transverse spiral becomes conical ($m_x\neq 0$), it is possible to observe structural reflections also at τ.[7] This means that first harmonic reflections can have a mixed magnetic and lattice character. Indeed we have ob-

 ©2008 The American Physical Society

served in magnetic fields the $\delta^{Mn}\mathbf{b}^*$ reflection in nonresonant x-ray diffraction experiments[9] for $\mu_0 H > 1$ T. Therefore the investigation of incommensurate reflections in multiferroic manganites using x-ray diffraction can provide valuable information on the type of magnetoelastic coupling that can be active in these multiferroics.

More recently it was shown that in $TbMnO_3$, the magnetic ordering of Tb and Mn spins are highly coupled below T_s.[10] While for $T > T_s$ the magnetic wave vectors for Tb and Mn are locked so that $\tau^{Tb} = \tau^{Mn}$,[3] below T_N^{Tb} it is found that τ^{Tb} and τ^{Mn} lock in to wave vectors whose magnitudes are rational fractions $3/7\mathbf{b}^*$ and $2/7\mathbf{b}^*$, respectively, while the wave vectors hold the relationship $3\tau^{Tb} - \tau^{Mn} = 1$. This novel matching of wave vectors can be described within the frustrated Anisotropic-Next-Nearest-Neighbor-Ising (ANNNI) model coupled to a periodic external field produced by the Mn spin order, as detailed in Ref. 10. Within this model the $\tau^{Tb} = \tau^{Mn}$ behavior is recovered, while the $\tau^{Tb} = 3/7\mathbf{b}^*$ and $\tau^{Mn} = 2/7\mathbf{b}^*$ regime is stabilized by an optimal ordering of six domain walls in the Tb-spin density wave, superimposed on the Mn order. This model further shows that the ordering of $\tau^{Tb} = 3/7\mathbf{b}^*$ is energetically more favorable than the simple $\uparrow\uparrow\downarrow\downarrow$ with $\tau = 1/2\mathbf{b}^*$ found at low temperatures for $DyMnO_3$.[11]

In this paper we report on x-ray diffraction measurements of the lattice deformation in $TbMnO_3$ as a function of temperature and magnetic field applied parallel to the a and b axis. The paper is organized in the following way. In Sec. II we present the experimental setups used for the present investigations. In Sec. III we report on zero-field measurements as a function of temperature for selected 2τ reflections. In Sec. IV, we present measurements with magnetic field applied along the a^* direction and in Sec. V, with magnetic field applied along the b^* direction. The phase diagram resulting from our data is discussed in Sec. VI.

In this paper we follow the convention of labeling incommensurate magnetic reflections from Bertaut's representational theory.[12] Here the magnetic ordering of Mn spins within space group $Pbnm$ and $\tau^{Mn} = 0.27b^*$ can be described by four irreducible representations (Γ) that consist of four modes (labeled as A, C, F, and G).[12] The modes correspond to magnetic superlattice reflections that occur in different Brillouin zones with extinction conditions as follows; A for $h+k$=even, l=odd; G for $h+k$=odd with l=odd; F for $h+k$=even and l=even; and C for $h+k$=odd and l=even, where h, k, l are Miller indices. Each mode here describes the Mn spin polarization along one unique principle crystallographic axis.[12] It is shown that the Mn transverse spiral ordering in $TbMnO_3$ is described by two irreducible representations $\Gamma_2 \times \Gamma_3$, where $\Gamma_2 = (C_x, F_y, A_z)$ and $\Gamma_3 = (G_x, A_y, F_z)$.[3] The ordering of the Mn spins is described by two A modes, A_y, A_z.[3] Using a combination of unpolarized and polarized neutron diffraction and resonant magnetic x-ray scattering, it has been shown that the remaining modes arise from the ordering of Tb spins.[3,13] In the following, the notation $\tau^{Mn/Tb} = (0, \delta^{Mn/Tb}, 0)$ for first harmonic and $2\tau^{Mn/Tb} = (0, 2\delta^{Mn/Tb}, 0)$ for second harmonic Mn and Tb incommensurate superlattice reflections is used, with wave vector τ and wave number δ. In the intermediate and the commensurate phases, numerical values for wave numbers are used.

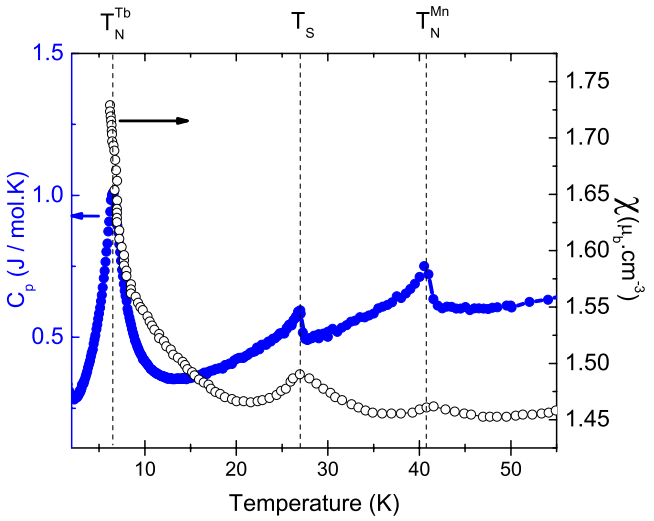

FIG. 1. (Color online) Temperature dependence of the specific heat (C_p) and magnetic susceptibility χ of a small single crystal from the $TbMnO_3$ boule. For the magnetization measurements a field of 0.01 T was applied along the c axis. The $C_p(T)$ and $\chi(T)$ data indicate three successive phase transitions at 7, 27, and 41 K corresponding to T_N^{Tb}, T_s, T_N, respectively.

II. EXPERIMENT

The $TbMnO_3$ crystals used in our experiments were grown at the Hahn-Meitner-Institute in Berlin using the floating zone technique under Ar atmosphere. The crystals cut from the crystalline boule show an excellent crystal quality with a mosaic spread of 0.016° of the (0 2 0) reflection [full width at half maximum (FWHM)]. In Fig. 1 we show measurements of the temperature dependence of heat capacity and magnetic susceptibility from a small single crystal cut from the same crystalline boule. The data shows three successive transitions with decreasing temperature at $T_N = 41$ K, $T_s = 28$ K, and $T_N^{Tb} = 7$ K. The measurements and transition temperatures are in good agreement with published measurements,[5] indicating a high quality crystal.

The experiments were performed both at the beamline BW5 at the Hamburger Synchrotronstrahlungslabor (HASYLAB) and at the beamline X21 at the National Synchrotron Light Source (NSLS) at Brookhaven National Laboratory. At HASYLAB the experiment was conducted at a photon energy of 100 keV in horizontal scattering geometry. The sample was mounted in a Cryogenics superconducting cryomagnet with horizontal field up to 10 T. The beam was monochromized by a (111)-SiGe gradient crystal. A second SiGe gradient crystal was used as analyzer to suppress background. The single crystalline $TbMnO_3$ sample had a size of $2 \times 3 \times 0.6$ mm^3 and was measured in transmission geometry, which means the true bulk of the crystal is probed. The sample thickness in the direction of the beam was of the order of the absorption length at this high x-ray energy and was thus optimum for obtaining maximum scattering intensity. The crystal was aligned with the bc plane in the horizontal diffraction plane in order to access $(0,k,l)$ reflections. Using this setup, measurements were performed with field $H \| b$. At NSLS, the experiment was conducted in

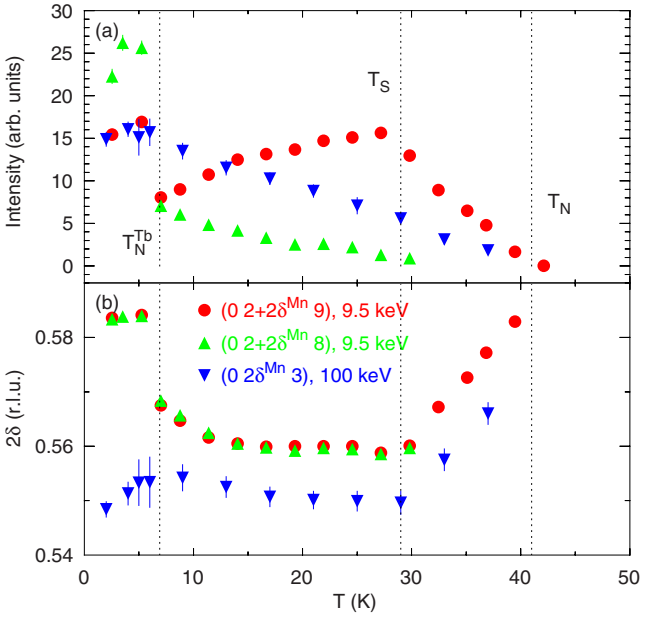

FIG. 2. (Color online) Temperature dependence at zero field and 9.5 keV photon energy of the (a) intensity and (b) k component of the wave vector of the A-mode $(0,2+2\delta^{\mathrm{Mn}},9)$ and F-mode $(0,2+2\delta^{\mathrm{Mn}},8)$ reflections. The respective temperatures T_N, T_s, and T_N^{Tb} are indicated by dashed lines. In addition data for the A-mode $(0,2\delta^{\mathrm{Mn}},3)$ reflection measured at 100 keV are plotted. Due to a systematic offset the absolute wave numbers are not accurate.

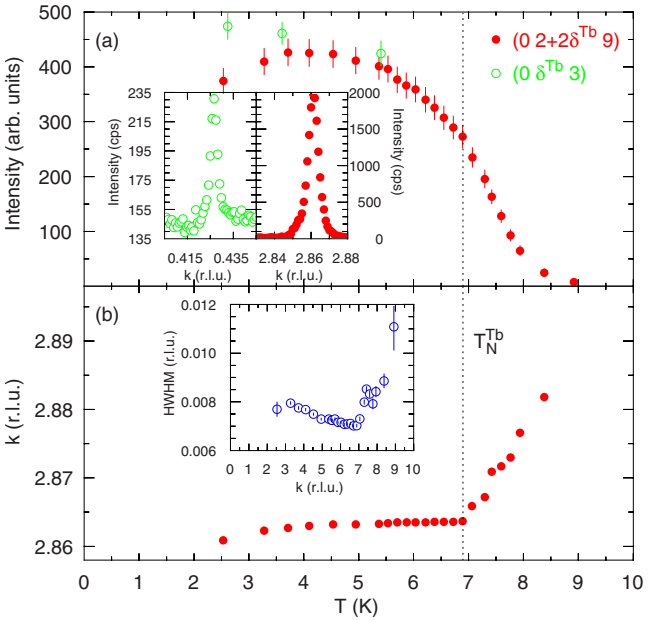

FIG. 3. (Color online) Tb-superlattice reflection as function of temperature. (a) shows the intensity of $(0,2+2\delta^{\mathrm{Tb}},9)$ and $(0,\delta^{\mathrm{Tb}},3)$. (b) shows the variation of the propagation vector of the $(0,2+2\delta^{\mathrm{Tb}},9)$ superlattice reflection. In the inset, a scan over the first- and second-harmonic peak along the b^* direction is shown.

the hard x-ray regime at 9.5 keV, as well as at the Tb L_2 absorption edge with a photon energy of 8.252 keV. The sample was mounted in a 13 T Oxford cryomagnet with vertical magnetic field. With this setup, measurements with field $H\|a$ were conducted, with the bc plane oriented in the horizontal diffraction plane.

A (002) graphite analyzer was used for background reduction for the non-resonant measurements. As detector, a field insensitive Avalanche Photodiode (APD) was used.

For measurements performed at the absorption edge, polarization analysis was performed using the (006) reflection of the graphite analyzer. The scattering geometry was $\pi-\sigma'$ with the analyzer at an angle of $2\theta_{(006)}=84.6°$, implying a leakage of less then 1% from the $\pi-\pi'$ channel. The sample used here was a crystal with polished c surface and a size of about 3×3 mm^2 in order to obtain high diffracted intensities in Bragg geometry.

All results presented in this study measured away from the resonances at the absorption edges are due to pure charge scattering. This can safely be assumed since the non-resonant magnetic scattering cross section is about six orders of magnitude weaker than the charge scattering cross section. Besides this, the magnetic signal of the observed reflections is further reduced due to the small magnetic form factor at the high Q values we investigate here.

III. MEASUREMENTS AT ZERO FIELD

In Fig. 2 we show the dependence of the intensity and wave vector with temperature of the A-mode $(0,2+2\delta^{\mathrm{Mn}},9)$ and F-mode $(0,2+2\delta^{\mathrm{Mn}},8)$ reflections measured using a photon energy of 9.5 keV. From this data it is clear that the variation of intensity of the two reflections with decreasing temperature is substantially different and reflects the origin of these reflections. The A mode reflects the lattice modulation that arises purely from the ordering of Mn spins, while the F mode reflects the lattice distortion that arises from the induced ordering of Tb spins with $\tau^{\mathrm{Tb}}=\tau^{\mathrm{Mn}}$. For the A-mode reflection with decreasing temperature below T_N, we find a linear increase in its intensity up to T_s, while below T_s its intensity decreases with further cooling down to T_N^{Tb}. As Tb spins order, the intensity of these reflections rapidly increases for $T<T_N^{\mathrm{Tb}}$. This is in sharp contrast to the F-mode reflection, where the intensity shows a smooth increase with decreasing temperature down to T_N^{Tb}, while a similar jump in intensity as for the A-mode reflections is observed below T_N^{Tb}. In Fig. 2 we show also data measured from the A-mode $(0,2\delta^{\mathrm{Mn}},3)$ reflection using 100 keV x rays. The behavior here is different to the 9.5 keV data. The intensity increases smoothly with temperature down to T_N^{Tb}, below which it saturates. No jump in intensity nor a jump of the wave vector at T_N^{Tb} is observed here. A possible scenario for the behavior of this reflection is presented at the end of this section.

In Fig. 3 we show detailed measurements of the $(0,2+2\delta^{\mathrm{Tb}},9)$ and $(0,\delta^{\mathrm{Tb}},3)$ reflections below $T_N^{\mathrm{Tb}}=9$ K that describe the lattice modulation associated with the change of the Tb ordering from $\tau^{\mathrm{Tb}}=\tau^{\mathrm{Mn}}$ to $3\tau^{\mathrm{Tb}}-\tau^{\mathrm{Mn}}=1$.[10] The intensity of the $2\tau^{\mathrm{Tb}}$ reflection shows a typical order parameters behavior with cooling below T_N^{Tb} that follows the ordering of Tb spins. Below 6 K we can also measure the first harmonic $(0,\delta^{\mathrm{Tb}},3)$ reflection [Fig. 3(b)] that is visible with non-resonant x-ray scattering, showing that below T_N^{Tb} there is a structural component to the first-harmonic magnetic reflec-

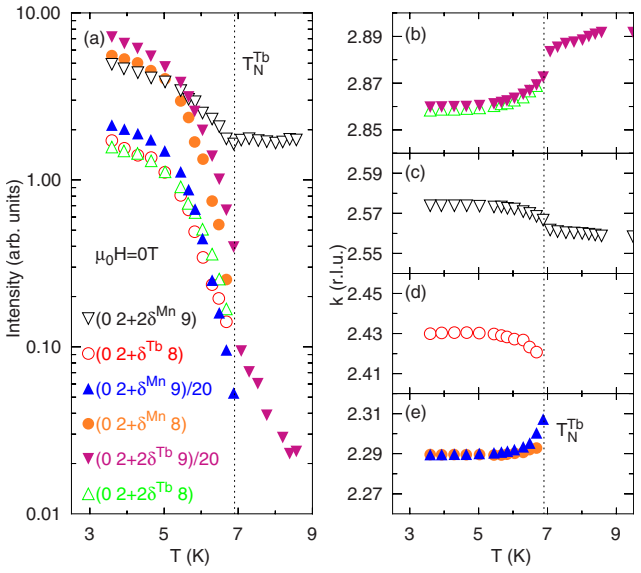

FIG. 4. (Color online) Temperature dependence of (a) intensities and [(b)–(e)] wave number of the first- and second-harmonic structural Mn- and Tb-superlattice reflections in the Tb-ordered phase $T<T_N^{Tb}$ at zero field.

tion. This is supported by the observation of a strong first-harmonic Tb reflection shown in Fig. 4.

The variation with temperature for the wave vectors $2\tau^{Mn}$ and $2\tau^{Tb}$ is shown in Figs. 2(b) and 3(b), respectively. We find that the value of $2\delta^{Mn}$ rapidly decreases on cooling through the SDW regime as noted earlier and shows a weaker temperature dependence below T_s.[3] However at T_N^{Tb} we note a substantial increase in the value of $2\delta^{Mn}$ that tracks closely the rapid changes in δ^{Tb} between 9 and 7 K, while below 7 K the values of both incommensurabilities remain relatively temperature invariant. Below T_N^{Tb} we confirm the observation that the wave vectors for Mn- and Tb-spin orders are coupled. Indeed the wave vectors of $(0,2+2\delta^{Tb},9)$ and $(0,2+2\delta^{Tb},8)$, as well as $(0,2+\delta^{Mn},8)$ and $(0,2+\delta^{Mn},9)$ in Figs. 4(b)–4(e) are following the relation $3\tau^{Tb}-\tau^{Mn}=1$. Below 5 K the respective wave numbers approach the values of $\delta^{Mn}=2/7$ and $\delta^{Tb}=3/7$ within 0.002 accuracy, as was shown to be the case in Ref. 10.

We note here that we found surprising differences in the change of the value of δ^{Mn} through the transition at T_N^{Tb}. Through this transition Kenzelmann *et al.* (Ref. 3) report a jump in δ^{Mn} of $\sim 10^{-3}$ using single-crystal neutron diffraction. This value is similar to the neutron measurements reported in Ref. 13, as well as x-ray diffraction measurements using 100 keV x rays shown for the $(0,2\delta^{Mn},3)$ reflection in Fig. 2(b). This is in contrast to the $\sim 10^{-2}$ change we find across T_N^{Tb} using 9.5 keV x rays in this work [Fig. 2(b)], as well as in Ref. 10. In the case of the 9.5 keV experiments, we probe few micrometers of the surface of the crystal, while in the neutron and high-energy x-ray experiments we probe the bulk of the sample. This one order of magnitude difference in the change of δ^{Mn} across T_N^{Tb} suggests that strain effects at the crystal surface allows the lock-in of the wave vectors to values of rational fractions within $\Delta\delta\sim 10^{-2}$, while the unstrained bulk appears to modulate the values of the wave vectors below T_N^{Tb}.

We now turn our attention to the intensity variation with temperature of the *A*- and *F*-mode $2\tau^{Mn}$ reflections shown in Fig. 2. The behavior of the *A*-mode $(0,2+2\delta^{Mn},9)$ reflection can be understood in terms of the changes in the magnetic ordering of Mn spins. In the SDW regime between $T_s<T<T_N$, the increase in intensity of the $2\tau^{Mn}$ *A* mode arises from the quadratic magnetoelastic coupling, in which the amplitude of the lattice displacements varies linearly with the increase in the size of ordered Mn moment.[6,7] The decrease in intensity below T_s is ascribed to the development of a perpendicular component that alters the collinear SDW to a transverse spiral.[7] For a perfect spiral with $m_y=m_z$, the $2\tau^{Mn}$ reflection would be completely suppressed;[7] however our data shows that at a temperature just above T_N^{Tb}, the $2\tau^{Mn}$ reflection is still observed, indicating that the spiral remains elliptical $(m_y\neq m_z)$. Indeed this is confirmed by neutron diffraction by measuring directly the values of m_y and m_z to be 3.9 and 2.8 μ_B/Mn, respectively.[3] At T_N^{Tb} the intensity of the $2\tau^{Mn}$ *A* mode jumps dramatically. At first glance this rise in intensity may suggest changes in the magnetoelastic coupling of Mn and Tb sublattices. However, more likely the jump in intensity below T_N^{Tb} arises from the matching of the Mn and Tb wave vectors as described above. Since we know that below T_N^{Tb} we have significant structural contribution to the magnetic τ^{Tb} reflections, it is most likely that here the τ^{Tb} intensity is superimposed on a $2\tau^{Mn}$ reflection below T_N^{Tb} and thus providing dramatic changes in intensity.

More puzzling is the difference in behavior of the *A*-mode reflections measured with 9.5 keV and 100 keV x rays, which are also shown in Fig. 2, where the 100 keV data show a linear variation in intensity with cooling from T_N down to T_N^{Tb}, in contrast to the behavior observed for 9.5 keV photons. Here again, we believe this has to do with surface versus bulk properties of the material, since also measurements performed with bulk sensitive neutron scattering show the behavior of the *A*-mode reflections, we observe here with high-energy x rays.[3,14]

IV. FIELD ORIENTATION $H\|a$

The application of magnetic field along the *a* axis results in strong modulations of the magnetic order of Tb and Mn spins with the consequence of affecting significantly the ferroelectric properties. The most notable change with field is the flop of the direction of the spontaneous polarization from $P\|c$ to $P\|a$. Phenomenologically this is attributed to the flop of the Mn spin spiral from the *bc* plane to the *ab* plane. This flop is accompanied by a change of τ^{Mn} to a commensurate value of 1/4 at a critical field H_C^a of approximately 10 T at 2 K.[9] In this section we focus predominantly on field-induced magnetoelastic transitions that occur below H_C^a and give us an insight into both the magnetic ordering and magnetoelastic coupling in $TbMnO_3$.

A. Phase region $T_N^{Tb}<T<T_N^{Mn}$

We measured the field dependence for $H\|a$ for τ and 2τ reflections at $T=27$, 15, and 9 K. In Figs. 5(a)–5(d), we show the field dependence at $T=27$ and 15 K, below T_s, for the

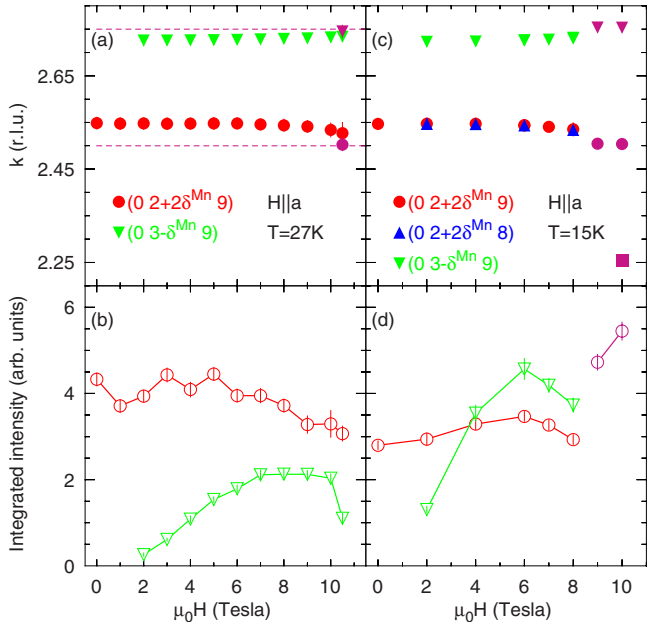

FIG. 5. (Color online) Magnetic-field dependence of (a) wave vector and (b) intensity of the second-harmonic $(0,2+2\delta^{\mathrm{Mn}},9)$ (circles) and first-harmonic $(0,3-\delta^{\mathrm{Mn}},9)$ (triangles) superlattice reflection at a sample temperature of $T=27$ K for $H\|a$. Magnetic-field dependence of (c) wave vector and (d) intensities of the CM and IC superlattice reflection for magnetic field $H\|a$ at a sample temperature $T=15$ K. At $\mu_0 H_C^a=9$ T the reflections lock in at CM positions. The horizontal dashed lines show the half and quarter integer positions of the CM first- and second-harmonic reflections above H_C^a.

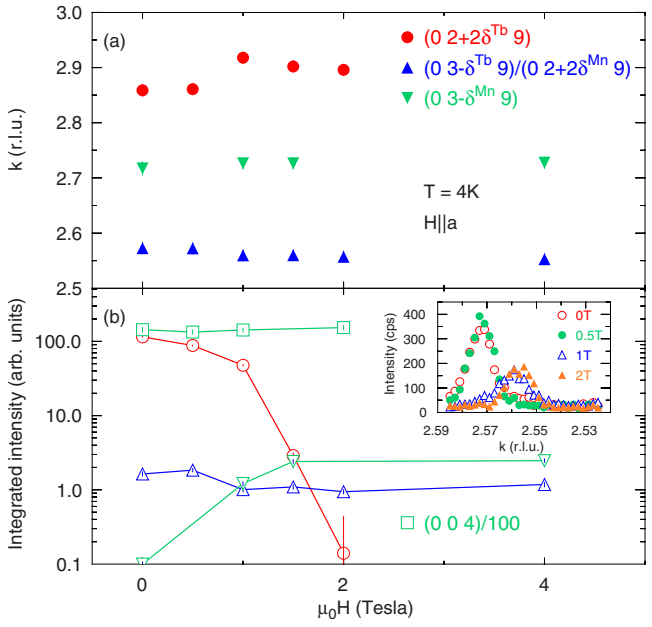

FIG. 6. (Color online) Field dependence at $T=4$ K of the terbium and manganese superlattice reflections with magnetic field $H\|a$. (a) peak positions (closed symbols) and (b) the corresponding intensities (open symbols) are shown. Open rectangles show the (0, 0, 4) main Bragg intensity divided by a factor 100. The inset in (b) shows the peak profiles of the $(0,3-\delta^{\mathrm{Tb}},9)$ and $(0,2+2\delta^{\mathrm{Tb}},9)$ reflections for different fields.

A-mode $2\tau^{\mathrm{Mn}}$ reflection $(0,2+2\delta^{\mathrm{Mn}},9)$ and the F-mode $(0,2+2\delta^{\mathrm{Mn}},8)$ reflection for 15 K only. In this regime Tb and Mn spins are ordered with the same wave vector ($\tau^{\mathrm{Mn}}=\tau^{\mathrm{Tb}}$). The τ^{Mn} and $2\tau^{\mathrm{Mn}}$ reflections for the C and G modes are too weak to be observed at these two temperatures.

The intensity of the $2\tau^{\mathrm{Mn}}$ A and F modes for $T=27$ and 15 K is essentially constant with increasing field up to H_C^a, suggesting that field does not change either the ellipticity of the Mn spin-spiral or the magnetoelastic coupling associated with it. Surprisingly above 2 T for both 27 and 15 K, we observe the τ^{Mn} G-mode $(0,3-\delta^{\mathrm{Mn}},9)$ reflection. The wave number of this reflection is $\delta^{\mathrm{Mn}}=0.275$ at $\mu_0 H=2$ T, in agreement with the incommensurability $2\delta^{\mathrm{Mn}}=0.55$ of the $2\tau^{\mathrm{Mn}}$ reflection. The intensity of this reflection shows a linear increase with field above 2 T and saturates at approximately 6 T [Figs. 5(b) and 5(d)]. Similar measurements as a function of field at 9 K just above T_N^{Tb} show the very same behavior as described above for the same reflections. Additional scans (not shown) demonstrate that only τ^{Mn} G and C modes are observed above 2 T, while the $2\tau^{\mathrm{Mn}}$ A and F modes are always measurable irrespective of field. The observation of τ^{Mn} reflections in fields larger than 2 T may have a number of possible reasons. The emergence of a first-harmonic reflection may be thought at first glance as trivial as the coupling of the lattice to H becomes linear. However Jia *et al.*[7] suggest that a linear behavior to the spin-lattice coupling may occur in the case when the transverse spiral becomes conical, i.e., $m_x \neq 0$. If this was indeed true then we would expect to observe the τ^{Mn} reflection of an A mode as such a reflection describes the Mn spiral ordering. However according to our observations the first-harmonic reflections in field are found for G and C modes, suggesting possible changes to the Tb-spin ordering with magnetic field. Indeed magnetization measurements in Ref. 15 suggest the ferromagnetic alignment of Tb spins with $H\|a$ for $T=15$ and 9 K. Therefore the emergence of τ^{Mn} reflections with field most likely is associated with changes in the Tb ordering, as opposed to changes in the magnetoelastic coupling.

B. Phase region $T<T_N^{\mathrm{Tb}}$

We now turn our attention to the behavior of the incommensurate reflections as a function of field below T_N^{Tb} and remind the reader that in this regime at zero field, the Tb and Mn magnetic ordering is coupled so that $3\tau^{\mathrm{Tb}}-\tau^{\mathrm{Mn}}=1$. As shown Fig. 6 we find τ^{Tb} and the A-mode τ^{Mn} for $\mu_0 H=1$ T and $T<T_N^{\mathrm{Tb}}$. Increasing magnetic field results in the strong attenuation of the $2\tau^{\mathrm{Tb}}$ $(0,2+2\delta^{\mathrm{Tb}},9)$ reflection and its complete suppression above $\mu_0 H>2$ T, consistent with the FM ordering of Tb spins as indicated by neutron diffraction.[9]

For intermediate field values ($0<H<2$ T), the $2\tau^{\mathrm{Tb}}$ reflection vanishes from the $2\delta^{\mathrm{Tb}}=0.86$ position and seems to shift to 0.90 (Fig. 6). On the other hand resonant scattering from the Tb L_2 absorption edge indicates a shift of the first-harmonic τ^{Tb} reflection to 0.364, indicating a shift of the $2\tau^{\mathrm{Tb}}$ reflection to the 0.727 position, where also a peak appears at ≈ 1 T, as will be shown later. This reflection never-

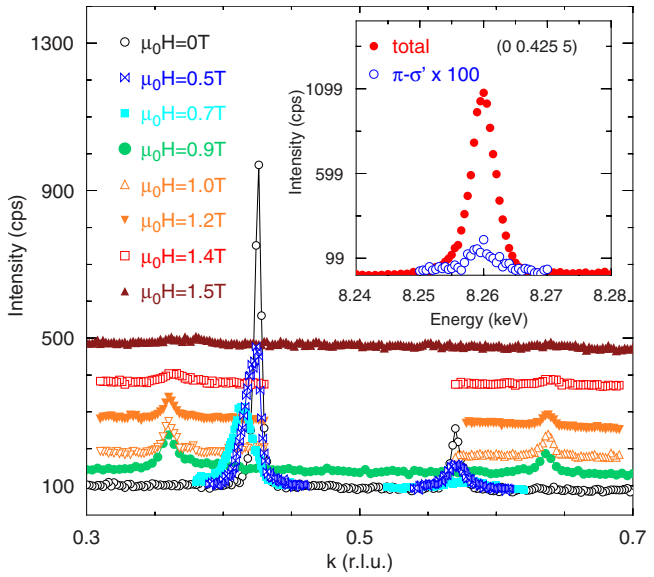

FIG. 7. (Color online) K scans of the $(0,\delta^{\mathrm{Tb}},5)$ and $(0,1-\delta^{\mathrm{Tb}},5)$ reflection as function of field $H\|a$ at a sample temperature $T=4$ K without polarization analysis. The inset shows an energy scan over the Tb L_2 absorption edge with and without polarization analysis in the $\pi-\sigma'$ channel. The total signal only shows the resonant intensity. The fluorescence background is subtracted using an energy scan performed off the reflection position.

theless stays also above a field of 2 T, which indicates that we deal here with the τ^{Mn} reflection observed also at temperatures $T>T_N^{\mathrm{Tb}}$. The shift observed at 1 T is coupled to a discontinuous change in the $2\delta^{\mathrm{Mn}}$ reflection from 0.572 to 0.56 also for the same field values as shown in the inset of Fig. 6(b). This again is due to the superposition of the τ^{Tb} intensity on the $2\tau^{\mathrm{Mn}}$ reflection at low fields and a pure $2\tau^{\mathrm{Mn}}$ reflection at higher fields.

To investigate the transition to this intermediate phase, we performed resonant x-ray diffraction measurements with and without polarization analysis in the $\pi-\sigma'$ polarization channel as a function of $H\|a$ by tuning the photon energy to the Tb L_2 edge at 8.252 keV. At this photon energy, the background was significantly higher than for the experiments at 9.5 keV and prohibited the observation of any non-resonant scattering signal. However, a strong resonant magnetic signal was observed at $T=4$ K for the first-harmonic Tb reflections $(0,k\pm\delta^{\mathrm{Tb}},l)$ with l=odd (Tb magnetic A and C modes). The measurements were conducted with analyzer used to reduce background [PG(002)] and as polarization analyzer [PG(006)] for the $\pi-\sigma'$ channel. In the inset of Fig. 7, energy scans with and without polarization analysis are shown. The small intensity in the $\pi-\sigma'$ channel is due to leakage since the analyzer angle is not exactly at $2\theta=90°$ but at $2\theta_{(006)}=84.6°$. All intensity is thus scattered in the $\pi-\pi'$ channel. According to the resonant magnetic-scattering cross section, this is the case if the magnetic Tb moment is aligned along the a^* direction perpendicular to the scattering plane, consistent with results in Ref. 16.

In Fig. 7 scans over the $(0,\delta^{\mathrm{Tb}},5)$ and $(0,1-\delta^{\mathrm{Tb}},5)$ positions with $\delta^{\mathrm{Tb}}=0.43$ are shown as function of field. As the field is increased, the intensity of these reflections decreases, and the wave number δ^{Tb} slightly shifts as observed in the non-resonant experiment. At $\mu_0H=0.9$ T, this resonant reflection shifts discontinuously from $\delta^{\mathrm{Tb}}=0.428(2)$ ($\mu_0H=0$ T) to $\delta^{\mathrm{Tb}}=0.363(1)$ ($\mu_0H=1$ T). While the wave number of this reflection is invariant in field, its intensity is rapidly reduced with increasing field and vanished above $H\|a=2$ T, when Tb spins show a FM ordering ordering.[13] Our resonant and non-resonant measurements demonstrate that this intermediate phase is stable between $H\|a=0.9$ and 2 T.

The discontinuous transition we find here at 1 T suggests a change in the coupling of the Mn and Tb ordering. In this new regime the values of δ^{Tb} and δ^{Mn} are close to the rational fractions 4/11 and 3/11, respectively, while the wave vectors hold the relationship of $2\tau^{\mathrm{Tb}}+\tau^{\mathrm{Mn}}=1$ with 0.001 accuracy. Modeling of the Mn and Tb spins using an ANNNI model, it was shown that such a state is stabilized as the Tb-SDW acquires a homogeneous component via χH and couples to the quartic term of the Landau expansion.[10] Interestingly the change in the coupling between Mn and Tb magnetic ordering characterizes a region in which the value of $P\|c$ increases by ~30% up to $H\|a=2$ T.

For $H\|a>2$ T the FM alignment of Tb spins results in the melting of the incommensurate Tb ordering.[9,13,15] This melting is associated with a decrease in $P\|c$ to values 30% smaller than the maximum polarization at zero field. However τ^{Mn} and $2\tau^{\mathrm{Mn}}$ reflections are observed above 2 T and discontinuously shift to values of 1/4 and 1/2, respectively, at H_C^a (not shown).

V. FIELD ORIENTATION $H\|b$

Whereas the $H\|a$ measurements were performed with photon energies of 9.5 keV that allows to probe only the first few micrometers of the crystal, the measurements with $H\|b$ are performed with high photon energies of 100 keV, with which the true bulk of the crystal is probed. For the $H\|b$ geometry the sequence of magnetostructural transitions toward the polarization flop transition is significantly different than what we have found for the $H\|a$ configuration. Although we find that the polarization flop again corresponds to a first-order transition to a commensurate phase with $\delta^{\mathrm{Mn}}=1/4$, the sequence of transitions associated with Tb ordering differs from the $H\|a$ case. A summary of our results with respect to the wave numbers δ^{Mn} and δ^{Tb} is shown in Figs. 8(a)–8(c) for $T=2$, 10, and 20 K, respectively. The transition to $\delta^{\mathrm{Mn}}=1/4$ is clearly evident from the data while H_C^b decreases with decreasing temperature to values that agree well with the observation of the flop in polarization from $P\|c$ to $P\|a$.[5,15,17]

A. Phase region $T_N^{\mathrm{Tb}}<T<T_N^{\mathrm{Mn}}$

In the region of $T_N^{\mathrm{Tb}}<T<T_N$, we find only reflections with $2\tau^{\mathrm{Mn}}$ as expected from previous measurements and indicative of quadratic magnetoelastic coupling. However above $H_C^b>1$ T we find also first-harmonic reflection such as the F mode $(0,\delta^{\mathrm{Mn}},4)$. This reflection that arises from the ordering of Tb spins with $\tau^{\mathrm{Tb}}=\tau^{\mathrm{Mn}}$ shows a linear increase in intensity with fields up to H_C^b, indicating changes in the mag-

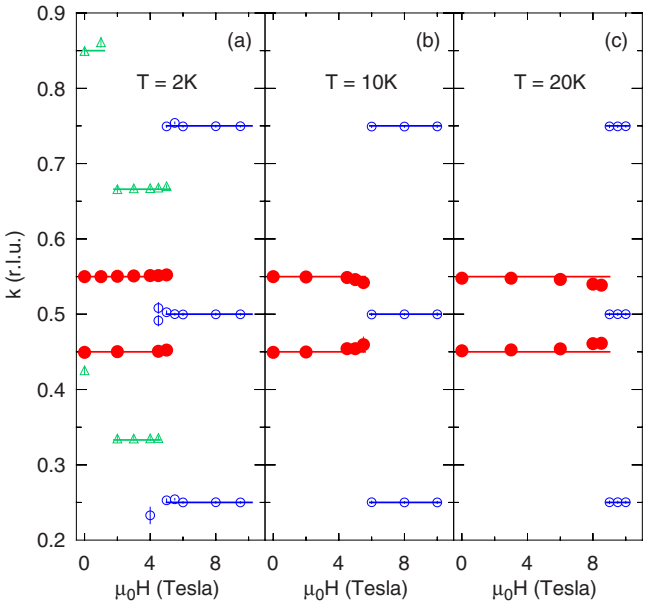

FIG. 8. (Color online) Incommensurability δ of the superlattice reflections $(0,2\delta^{\mathrm{Mn}},4)$ and $(0,1-2\delta^{\mathrm{Mn}},4)$ below H_C^b (closed circles) and (0, 0.25, 4), (0, 0.5, 4), and (0, 0.75, 4) above H_C^b (open circles), measured at (a) $T=2$ K, (b) $T=10$ K, and (c) $T=20$ K as function of magnetic field $H\|b$. At $T=2$ K in addition $(0,\delta^{\mathrm{Tb}},5)$ and $(0,2\delta^{\mathrm{Tb}},5)$ reflections are shown below and above H_C^{Tb} (open triangles).

netic ordering of Tb spins. In contrast its second-harmonic counterpart $(0,2\delta^{\mathrm{Mn}},4)$ remains constant in intensity up to H_C^b [Fig. 9(a)]. This linear increase over the whole field range is different from the behavior found for $H\|a$ (Sec. IV), where the intensity of these reflections increases initially but then decreases again toward H_C^a.

As we approach the critical field H_C^b, the value of $2\tau^{\mathrm{Mn}}$ begins to move toward 1/2, while at H_C^b we find a first-order

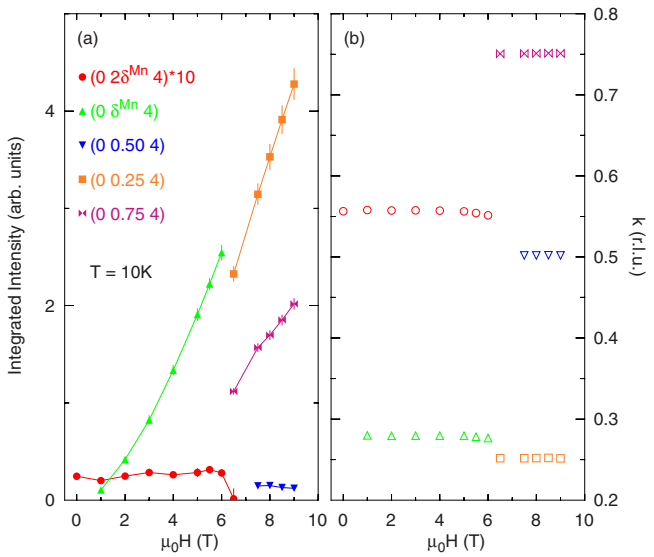

FIG. 9. (Color online) (a) Intensities as function of field of the IC $(0,\delta^{\mathrm{Mn}},3)$ and $(0,2\delta^{\mathrm{Mn}},4)$ reflections below H_C^b and the CM (0, 0.25, 4), (0, 0.5, 4), and (0, 0.75, 4) above H_C^b. (b) The respective wave vectors (0 k 4) for the intensities in (a) are shown.

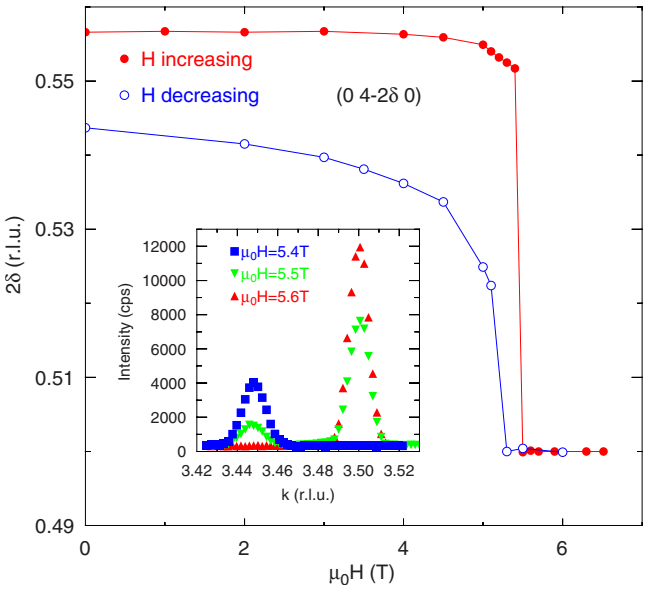

FIG. 10. (Color online) Hysteresis of the superlattice reflections measured at $T=10$ K. Solid circles show the data measured with increasing field, open circles the data measured with decreasing field. The inset shows the superlattice reflections at the phase transition for increasing field.

phase transition where the intensity of the incommensurate reflection decreases with field and vanishes as the commensurate reflection appears [Fig. 9(b)]. With decreasing temperature the value of H_C^b also decreases as shown in Figs. 8(a)–8(c). These changes to τ^{Mn} and $2\tau^{\mathrm{Mn}}$ F-mode reflections have to be attributed to changes in the magnetic structure associated with Tb spins. We speculate that at this high temperature, the application of magnetic field may result in the polarization of the Tb spins along the b axis. For this field direction there is no evidence of ferromagnetic ordering of Tb spins as found for $H\|a$.[5,13,15]

Detailed measurements of the transition to the commensurate phase were made at 10 K by tracking the lattice modulation associated with the F-mode structural peak $(0,4-2\delta^{\mathrm{Mn}},0)$. These measurements, shown in Fig. 10, were taken by cooling the sample to 10 K in zero field and applying field up to $H\|a=6.5$ T and then down to 0 T while the data were measured. These data show a hysteresis in terms of field and wave number $2\delta^{\mathrm{Mn}}$ that tracks the hysteresis in the polarization flop from $P\|c$ to $P\|a$.[5,15] In terms of magnetic field the hysteresis is as small as ~0.2 T. However in terms of wave number the effect is more pronounced. For increasing field the wave number remains at a value of $2\delta^{\mathrm{Mn}}=0.557$ almost up to H_C^b, before it locks to the commensurate value of 1/2. For decreasing field, a rapid increase in $2\delta^{\mathrm{Mn}}$ just below H_C^b and a significantly lower value of $2\delta^{\mathrm{Mn}}=0.543$ at $\mu_0 H=0$ T is observed. Interestingly, these lower values suggest $\delta^{\mathrm{Mn}}=0.272$, which is close to the rational fraction 3/11 as found for the case of $H\|a$ and 9.5 keV photons below T_N^{Tb}. In the inset of Fig. 10, scans over the superlattice reflections for increasing field around H_C^b are displayed. It shows the coexistence of the incommensurate and commensurate phase right at the transition at $\mu_0 H_C^b=5.5$ T. The intensities of these reflections in the incommensurate

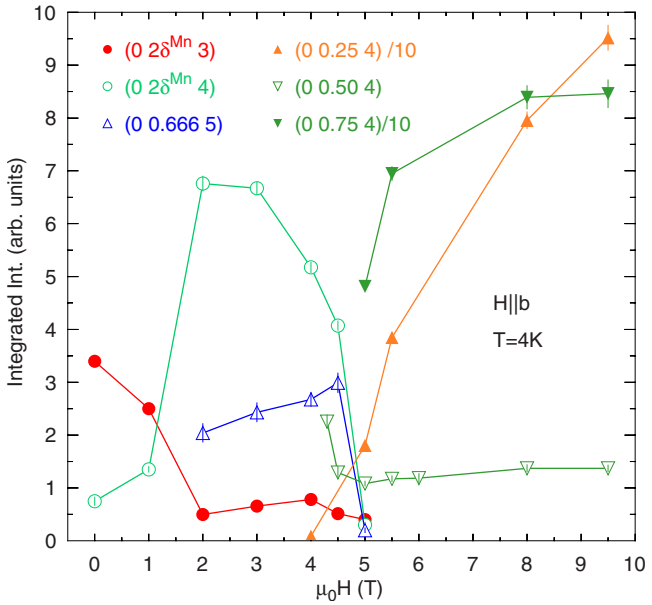

FIG. 11. (Color online) Intensities of the (0 0.55 3), (0 0.55 4), and (0 0.66 5) reflections below H_C^b and (0 0.25 4) and (0 0.5 4) above H_C^b as function of magnetic field $H\|b$ measured at a sample temperature of $T=4$ K.

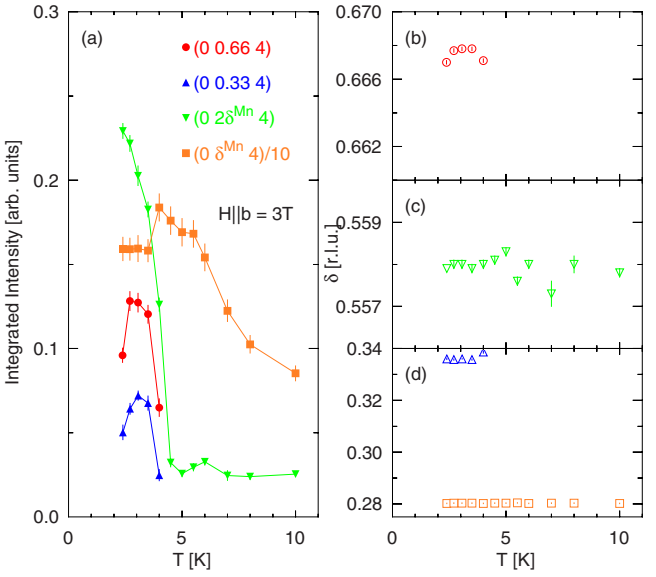

FIG. 12. (Color online) (a) Temperature dependence of the intensities of the Mn and Tb first- and second-harmonic superlattice reflections measured at magnetic field $\mu_0 H=3$ T. (b) Shows the corresponding k components of the wave vector. The measurement is performed by going from the intermediate Tb-ordered phase through T_N^{Tb} into the purely Mn ordered phase.

phase for increasing and decreasing field show exactly the same values while only their positions show hysteresis.

B. Tb-ordered phase region $T<T_N^{\mathrm{Tb}}$

The application of magnetic field at low temperature for the $H\|b$ configuration results in a significantly different behavior of τ^{Tb} and τ^{Mn} compared to the $H\|a$ configuration. Here the sample was cooled to 2 K in zero field and then data were measured with increasing field up to $\mu_0 H\|a=10$ T [Fig. 8(a)]. Between an applied field of 1 and 2 T, a phase transition is observed in the Tb sublattice with a shift of the peak positions from the incommensurate value $\tau^{\mathrm{Tb}}=0.43b^*$ to the commensurate value $\tau^{\mathrm{Tb}}=1/3b^*$ and accordingly from $2\tau^{\mathrm{Tb}}=0.86b^*$ to $2\tau^{\mathrm{Tb}}=2/3b^*$. Although this transition is only related to the Tb order, the intensities of the Mn reflections are influenced by this transition, whereas the wave vectors are not affected. As shown in Fig. 11, the intensities of the (0, 0.55, 3) (A mode) and the (0, 0.55, 4) (F mode) reflections show a distinct behavior. While the (0, 0.55, 3) intensity decreases at H_C^{Tb}, the (0, 0.55, 4) intensity increases.

Cooling the sample in an applied field $\mu_0 H=3$ T, we find in the temperature dependence that the transition to the incommensurate phase with $\tau^{\mathrm{Tb}}=0.43b^*$ is suppressed at $T_N^{\mathrm{Tb}}=4.5$ K with decreasing temperature in preference for the commensurate $\tau^{\mathrm{Tb}}=1/3b^*$ phase (Fig. 12). For the F-mode reflections $(0,\delta^{\mathrm{Mn}},4)$ and $(0,2\delta^{\mathrm{Mn}},4)$, we find no changes in the value of δ^{Mn} but again a clear change in the intensity is observed at T_N^{Tb}.

In this field-cooled measurement below $T=6$ K, we find two previously unreported modulations at (0, 0.298, 5) and (0, 0.6, 5). The nature of these reflections is not clear at this point, however their field dependence indicates that they are associated with Tb spin ordering. We find that increasing field and increasing temperature result in a considerable decrease in their intensity [Figs. 13(a) and 13(b)]. The reflections disappear at the transition to the $\delta^{\mathrm{Tb}}=1/3$ phase. Since these reflections only occur at the high-energy x-ray setup, they can be regarded as a bulk property related to Tb magnetic order below T_N^{Tb}.

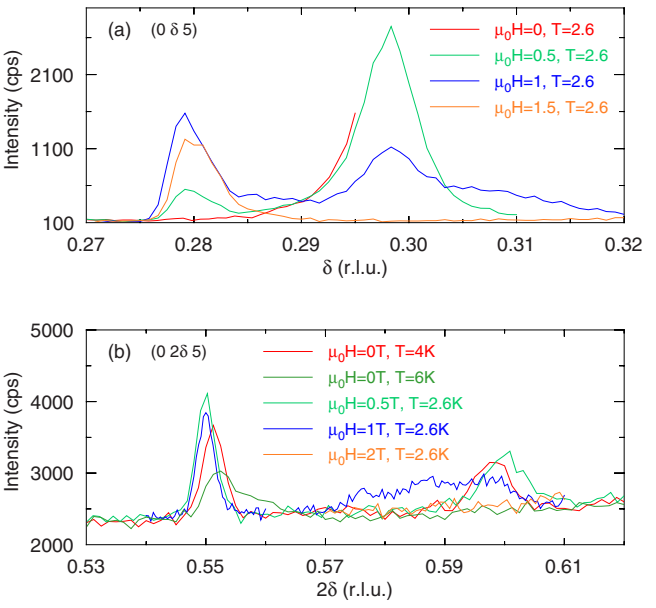

FIG. 13. (Color online) k scans over (a) $(0,\delta,5)$ and (b) $(0,2\delta,5)$ positions as function of magnetic field $H\|b$ and temperature below T_N^{Tb}.

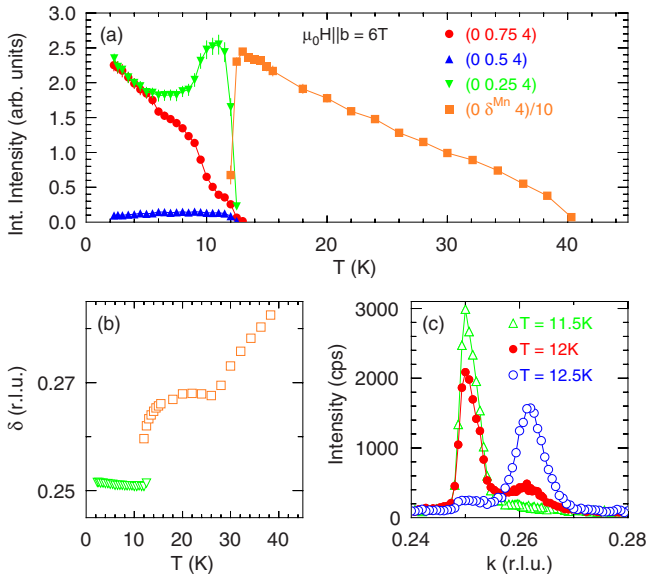

FIG. 14. (Color online) (a) Intensity behavior of CM and IC superlattice reflections measured at $H=6$ T below (CM) and above (IC) the critical temperature. (b) Corresponding wave number δ^{Mn} as function of temperature for the first-harmonic F-mode reflection. (c) k scans in the region of coexistence of the CM and IC phase at the critical temperature.

C. High-field commensurate phase

We now turn our attention to the commensurate phase above H_C^b. The scattering geometry that allows us to measure the commensurate phase makes only F and C modes accessible (Fig. 9). At $T=10$ K the transition to a commensurate phase occurs at $\mu_0 H_C^b=9$ T. Above H_C^b, the F and C modes exhibit a linear increase in their intensity with field for the first-harmonic reflections, whereas the intensity of the second-harmonic peaks remains constant with increasing field. This behavior follows on from the lower field behavior in the incommensurate phase. As the F and C modes arise from Tb ordering, it only allows us to comment on the value of τ^{Mn} and not to changes associated with the flop of the Mn spin spiral. Cooling the sample to $T=2$ K and applying field, we find the transition to the commensurate phase at $\mu_0 H_C^b=5$ T. Here reflections associated with the $\tau^{\mathrm{Tb}}=1/3b^*$ phase vanish at H_C^b, and only commensurate reflections with $\delta^{\mathrm{Mn}}=1/4$ and $2\tau^{\mathrm{Mn}}=1/2b^*$ are observed (Fig. 8). The integrated intensities of (0, 0.25, 4), (0, 0.5, 4), and (0, 0.75, 4) are plotted as function of $H\|b$ in Fig. 11. Intensities of the $2\tau^{\mathrm{Mn}}$ reflection are a factor of 30 weaker than the first harmonics. While the intensities of the (0, 0.25, 4) and (0, 0.75, 4) reflections increase linearly with field, the intensity of the (0, 0.5, 4) remains constant up to maximum field. The Tb (0, 0.66, 5) reflection also shows constant intensity from its onset at $\mu_0 H=2$ T up to H_C^b. At H_C^b a little intensity is still present and coexists with the reflections of the commensurate phase.

Following the F- and C-mode reflections while cooling the sample in a field $\mu_0 H=6$ T, we find that τ^{Mn} first takes an incommensurate value, which decreases with lowering the temperature until $T=T_s$ [see Figs. 14(a) and 14(b)]. Below T_s the value of τ^{Mn} remains relatively constant until approximately 18 K, where it rapidly decreases and locks into a value of $\tau^{\mathrm{Mn}}=1/4b^*$ below 12 K. In Fig. 14(c), k scans in the region of coexistence of the commensurate and incommensurate phase at the critical temperature are shown. The variation in the intensity of the commensurate reflections is quite different between the different reflections we examined. Whereas the weak second-harmonic reflection is constant in intensity, there is a strong variation for the first-harmonic reflections, indicating that changes in the Tb order obviously are still present even in the high-field commensurate phase.

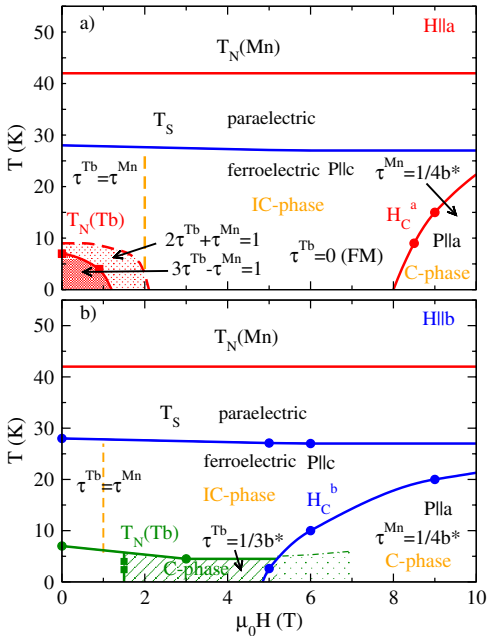

FIG. 15. (Color online) Phase diagram of $TbMnO_3$ for fields (a) $H\|a$ and (b) $H\|b$. In (a) the light-shaded area represents the intermediate phase region and the dark-shaded area, the Tb AF ordered state found for field $H\|a$. In (b) the green line represents T_N^{Tb} as found for magnetic field $H\|b$. The green shaded area shows the intermediate CM Tb-ordered phase for $H\|b$. The IC to CM transition for the manganese order is shown for $H\|a$ and $H\|b$. The vertical dashed line defines the onset of the first-harmonic reflections.

VI. PHASE DIAGRAM AND DISCUSSION

From the measurements we have described in this paper we can construct the $H-T$ phase diagrams for $H\|a$ and $H\|b$ [Figs. 15(a) and 15(b)], which summarize the various phases we have found and their correlation to the ferroelectric polarization of $TbMnO_3$ reported in Ref. 15.

In zero field we find purely structural $2\tau^{\mathrm{Mn}}$ reflections, which are interpreted to arise from quadratic magnetoelastic coupling. In the SDW regime $T_N>T>T_s$ the intensity of the A-mode $2\tau^{\mathrm{Mn}}$ reflections rises with cooling as expected for quadratic magnetoelastic coupling, and below T_s it decreases as the Mn magnetic order becomes spiral. While ideally $2\tau^{\mathrm{Mn}}$ reflections should disappear for a circular spiral,[7] their continual observation for $T>T_s$ reflects the ellipticity of the Mn spiral ordering.

In the regime $T_s > T > \tau^{Tb}$ Mn- and Tb-spin ordering is coupled and $\tau^{Mn} = \tau^{Tb}$.[10] Below T_N^{Tb}, Tb spins order with a different wave vector but remain harmonically coupled to the Mn spiral ordering as their wave vectors assume values that obey the relation $3\tau^{Tb} - \tau^{Mn} = 1$. This is confirmed in this work to an accuracy of 0.003 and we depict the phase regions of this coupled ordering in Figs. 15(a) and 15(b).

Application of magnetic field in this harmonically coupled state results in different behavior, depending on the direction of the field. When a relatively small magnetic field is applied along the *a* axis below T_N^{Tb}, we find an intermediate state that is characterized by the appearance of a Tb reflection at 0.9 [Figs. 4(b) and 6(a)], a jump of the wave vector τ^{Mn} to smaller values and a shift of τ^{Tb} to $0.36b^*$ observed by resonant magnetic scattering (Fig. 7). The observed shifts in wave vector are completely in agreement with the relationship $2\tau^{Tb} + \tau^{Mn} = 1$ (Secs. III and IV B) found in Ref. 10. This region is marked as a light shaded area in Fig. 15(a) and appears both in the temperature dependence at zero field (Fig. 4) between $T_N^{Tb} = 7$ K and ≈ 9 K, as well as in the field dependence at $T = 4$ K between 1 and 2 T (Fig. 6). For $\mu_0 H \| a > 2$ T Tb spins become ferromagnetically polarized. This intermediate phase may be visible only in the surface near region probed in this field configuration and is likely to be absent if the true bulk of the crystal is probed.

It is worth noting at this point that the intermediate value of τ^{Tb} below T_N^{Tb} for both $H \| a$ and $H \| b$ configurations is in fact quite similar; $\tau^{Tb} = 0.36b^*$ in the former case and $\tau^{Tb} = 0.33b^*$ for the latter. The difference in these two orderings of Tb spins is that for $H \| a$, τ^{Mn} is harmonically coupled to the Tb ordering while for $H \| b$ it is not. This subtle but significant difference we believe reflects the anisotropy of the Tb-spin ordering, as well as the delicate balance of the coupling between Mn and Tb spins.

When field is applied along the *b* axis below T_N^{Tb}, the harmonically coupled regime disappears, and instead we find a phase transition of the Tb moments at about $\mu_0 H = 1.25$ T from the incommensurate to a commensurate order with $\tau^{Tb} = 1/3b^*$ and the second-harmonic $2\tau^{Tb} = 2/3b^*$ [see Fig. 15(b)]. This intermediate Tb phase does not affect the wave vector τ^{Mn}, which only becomes commensurate at $\mu_0 5$ T. Nevertheless, intensities are affected, which emphasizes again the effect of the Tb magnetic order on the structure. Similar to $H \| a$, a dashed vertical line in Fig. 15(b) shows the field of onset for the first-order satellites, which are induced by the polarization of the Tb magnetic moment by the magnetic field. As discussed before (Sec. IV B) in the Tb-ordered region $T < T_N^{Tb}$ and the intermediate region ($\mu_0 H > 0$), a clear assignment of Mn or Tb reflections is no longer possible.

At higher field values for $\mu_0 H \| a > 2$ T and below T_s, only incommensurate Mn reflections with wave vectors τ^{Mn} and $2\tau^{Mn}$ are observed, whereas the Tb reflections disappear. Since first-harmonic reflections in field are found for *G* and *C* modes only and not for the Mn-order-related *A*-type reflections, this suggests that the vertical dashed line in Fig. 15(a) marks the onset of the FM order of the Tb moments for applied fields $H \| a$. This also corroborates neutron diffraction measurements, which find a sharp intensity decrease in the *F* and *C* modes in this field range and a sharp intensity increase in ferromagnetic Bragg reflections.[9] This FM ordering of Tb spins is relatively stable up to fields $H \| a > 8$ T.

For both field configurations $H \| a$ and $H \| b$, we find that the flop of the polarization is associated with a first-order transition to a commensurate $\tau^{Mn} = 1/4b^*$ phase. As the direction of the polarization changes, this flop is taken to reflect the flop of the spiral plane from the *bc* to the *ab* plane. The jump to a commensurate wave vector at the spiral flop transition is not surprising given that δ^{Mn} is in the proximity of a commensurate value in zero field, and therefore it is likely an energetically favorable state can be reached by a relative small shift to $\delta^{Mn} = 1/4$. This is in contrast to $DyMnO_3$ were the δ^{Mn} is not close to a commensurate value ($\tau^{Mn} = 0.38b^*$), and at the polarization flop transition the wave vector does not shift at all.[18] In $TbMnO_3$ above H_C^b, variations in Tb order seem still to be present, as can be deduced from the strong variation of the first-harmonic Mn reflections as function of temperature at a field of 6 T shown in Fig. 14. Here the transition of Tb ordering into the $\tau^{Tb} = 1/3b^*$ phase seems to extend into the commensurate phase above H_C^b, as is shown by the horizontal point-dashed line in Fig. 15(b).

In more general terms the flop of the polarization from $P \| c$ to $P \| a$ can be understood by the magnetic degrees of freedom of the Mn transverse spiral. There are three excitations of the spiral. One is the phase of the spiral polarized within the *bc* plane. Two other components are polarized along the *a* axis in zero field.[19] One of these components results in a flop of the *bc* spiral by a rotation around the *b* axis, while the other results in a twist of the spiral by a rotation around the *c* axis. All measurements thus far are consistent with the assumption that field applied either along the *a* or the *b* axis couples to the former mode and produces the flop of the spiral from the *bc* to the *ab* plane, while field applied along the *c* axis melts the spiral ordering.[20]

As this picture can describe the main flop of the polarization, as well as the magnetic excitations, this work has shown that the magnetic interactions between Mn and Tb spins remain significant and may be considered as a perturbation upon this model of the flop of the polarization and the spiral. The strength of he $J_{Mn\text{-}R}$ interaction can be gauged by noting that the flopping fields for the $R = Dy$ are lower than in the present case for $TbMnO_3$. This can be understood as a weaker $J_{Mn\text{-}R}$ for the case of $R = Dy$. Indeed in $DyMnO_3$ at low temperature, Dy spins become completely uncoupled from Mn spins and Dy orders with wave vector $\tau^{Dy} = 1/2\mathbf{b}^*$, a behavior significantly different from the harmonic coupling we find in $TbMnO_3$ below T_N^{Tb}.[10]

VII. CONCLUSIONS

In this paper we present an extensive study of the behavior of structural and magnetic superlattice reflections of $TbMnO_3$ as function of temperature and applied magnetic field. Details in the $H-T$ phase diagram are revealed by small changes in the magnitude of wave vector and intensities. These findings help us explain the changes in spontaneous polarization as function of temperature and field. The subtle difference in the Tb order wave vector observed at low

temperatures for nonzero fields $H\|a$ and $H\|b$ reflects the anisotropy of the Tb-spin order and the delicate balance between Mn and Tb spins. This again highlights the significance of interactions between Mn and Tb spins for the description of the polarization flop at the critical fields. Differences in the magnetic wave vector in the crystal bulk and the surface near region, as is observed by high-energy (100 keV) and hard x-ray investigations, show the influence of surface effects on magnetic polarization behavior in multiferroic compounds.

ACKNOWLEDGMENTS

We would like to thank W. Caliebe and C. S. Nelson for their assistance at the experiment at NSLS. Work at Brookhaven was supported by the U.S. Department of Energy, Division of Materials Science, under Contract No. DE-AC02-98CH10886. S.L. and D.N.A. were supported by the Deutsche Forschungsgemeinschaft under Contract No. AR-613/1-1.

*Joerg.Strempfer@desy.de

[1] T. Kimura, S. Ishihara, H. Shintani, T. Arima, K. T. Takahashi, K. Ishizaka, and Y. Tokura, Phys. Rev. B **68**, 060403(R) (2003).
[2] N. Hill, J. Phys. Chem. B **104**, 6694 (2000).
[3] M. Kenzelmann, A. B. Harris, S. Jonas, C. Broholm, J. Schefer, S. B. Kim, C. L. Zhang, S.-W. Cheong, O. P. Vajk, and J. W. Lynn, Phys. Rev. Lett. **95**, 087206 (2005).
[4] M. Mostovoy, Phys. Rev. Lett. **96**, 067601 (2006).
[5] T. Kimura, T. Goto, H. Shintani, K. Ishizaka, T. Arima, and Y. Tokura, Nature (London) **426**, 55 (2003).
[6] M. B. Walker, Phys. Rev. B **22**, 1338 (1980).
[7] C. Jia, S. Onoda, N. Nagaosa, and J. H. Han, Phys. Rev. B **76**, 144424 (2007).
[8] H. Katsura, N. Nagaosa, and A. V. Balatsky, Phys. Rev. Lett. **95**, 057205 (2005).
[9] N. Aliouane, D. N. Argyriou, J. Strempfer, I. Zegkinoglou, S. Landsgesell, and M. v. Zimmermann, Phys. Rev. B **73**, 020102(R) (2006).
[10] O. Prokhnenko, R. Feyerherm, M. Mostovoy, N. Aliouane, E. Dudzik, A. U. B. Wolter, A. Maljuk, and D. N. Argyriou, Phys. Rev. Lett. **99**, 177206 (2007).
[11] R. Feyerherm, E. Dudzik, N. Aliouane, and D. N. Argyriou, Phys. Rev. B **73**, 180401(R) (2006).
[12] E. F. Bertaut, J. Magn. Magn. Mater. **24**, 267 (1981).
[13] N. Aliouane, O. Prokhnenko, R. Feyerherm, M. Mostovoy, J. Strempfer, K. Habicht, K. C. Rule, E. Dudzik, A. U. B. Wolter, A. Maljuk, and D. N. Argyriou, J. Phys.: Cond. Mat. (to be published).
[14] R. Kajimoto, H. Yoshizawa, H. Shintani, T. Kimura, and Y. Tokura, Phys. Rev. B **70**, 012401 (2004).
[15] T. Kimura, G. Lawes, T. Goto, Y. Tokura, and A. P. Ramirez, Phys. Rev. B **71**, 224425 (2005).
[16] D. Mannix, D. F. McMorrow, R. A. Ewings, A. T. Boothroyd, D. Prabhakaran, Y. Joly, B. Janousova, C. Mazzoli, L. Paolasini, and S. B. Wilkins, Phys. Rev. B **76**, 184420 (2007).
[17] T. Arima, T. Goto, Y. Yamasaki, S. Miyasaka, K. Ishii, M. Tsubota, T. Inami, Y. Murakami, and Y. Tokura, Phys. Rev. B **72**, 100102(R) (2005).
[18] J. Strempfer, B. Bohnenbuck, M. Mostovoy, N. Aliouane, D. N. Argyriou, F. Schrettle, J. Hemberger, A. Krimmel, and M. v. Zimmermann, Phys. Rev. B **75**, 212402 (2007).
[19] D. Senff, P. Link, K. Hradil, A. Hiess, L. P. Regnault, Y. Sidis, N. Aliouane, D. N. Argyriou, and M. Braden, Phys. Rev. Lett. **98**, 137206 (2007).
[20] D. N. Argyriou, N. Aliouane, J. Strempfer, I. Zegkinoglou, B. Bohnenbuck, K. Habicht, and M. v. Zimmermann, Phys. Rev. B **75**, 020101(R) (2007).